Vibroacoustography for the assessment of total hip arthroplasty

Hermes A. S. Kamimura,[I,II] Liao Wang,[III,IV] Antonio A. O. Carneiro,[II] Randall R. Kinnick,[I] Kai-Nan An,[III] Mostafa Fatemi[I]

[I] College of Medicine, Mayo Clinic, Department of Physiology and Biomedical Engineering, Rochester/MN, USA. [II] Universidade de São Paulo, Faculdade de Filosofia, Ciências e Letras de Ribeirão Preto, Department of Physics, Ribeirão Preto/SP, Brazil. [III] Mayo Clinic, College of Medicine, Department of Orthopedics, Rochester/MN, USA. [IV] Shanghai Jiao Tong University School of Medicine and Engineering Research Center of Digital Medicine, Department of Orthopedics, Shanghai, China.

OBJECTIVES: This paper proposes imaging with 3-dimensional vibroacoustography for postoperatively assessing the uncovered cup area after total hip arthroplasty as a quantitative criterion to evaluate implant fixation.

METHODS: A phantom with a bone-like structure covered by a tissue-mimicking material was used to simulate a total hip arthroplasty case. Vibroacoustography images of the uncovered cup region were generated using a two-element confocal ultrasound transducer and a hydrophone inside a water tank. Topological correction based on the geometry of the implant was performed to generate a 3-dimensional representation of the vibroacoustography image and to accurately evaluate the surface. The 3-dimensional area obtained by the vibroacoustography approach was compared to the area evaluated by a 3-dimensional motion capture system.

RESULTS: The vibroacoustography technique provided high-resolution, high-contrast, and speckle-free images with less sensitivity to the beam incidence. Using a 3-dimensional-topology correction of the image, we accurately estimated the uncovered area of the implant with a relative error of 8.1% in comparison with the motion capture system measurements.

CONCLUSION: Measurement of the cup coverage after total hip arthroplasty has not been well established; however, the covered surface area of the acetabular component is one of the most important prognostic factors. The preliminary results of this study show that vibroacoustography is a 3-dimensional approach that can be used to postoperatively evaluate total hip arthroplasty. The favorable results also provide an impetus for exploring vibroacoustography in other bone or implant surface imaging applications.

KEYWORDS: Arthroplasty; 3D Imaging; Vibroacoustography.

Kamimura HA, Wang L, Carneiro AA, Kinnick RR, An KN, Fatemi M. Vibroacoustography for the assessment of total hip arthroplasty. Clinics. 2013;68(4):463-468.

Received for publication on October 15, 2012; **First review completed on** November 13, 2012; **Accepted for publication on** December 6, 2012

E-mail: fatemi.mostafa@mayo.edu

Tel.: 507284-0608

INTRODUCTION

Total hip arthroplasty (THA) is a cost-effective procedure to treat patients with end-stage osteoarthritis. The acetabular component may not obtain full coverage in patients with developmental dysplasia of the hip or in patients undergoing a revision procedure. Previous studies have investigated the relationship between the loosening rate and the measured cup coverage using plain anteroposterior pelvis radiographs, and the recommendations from these studies regarding adequate cup coverage have varied from 60% to 80% (1-4). However, the minimum requirement of 3-dimensional (3D) cup coverage, which can be used as a criterion during cup placement, is still under investigation (5). To provide precise information on the relationship between minimum cup coverage and the cup loosening rate, a noninvasive 3D imaging technique is required to postoperatively measure cup coverage. In this paper, we describe using vibroacoustography (VA) as a noninvasive tool for 3D imaging and for evaluating the uncovered area of the cup in THA.

VA is an ultrasound-based technique in which two cofocused ultrasound beams at slightly different frequencies (in the MHz range) generate low-frequency (in the kHz range) acoustic excitation caused by the radiation force of the interacting ultrasound beams (6,7) and the nonlinear mixing of the scattered waves (8). Recent studies have shown that the nonlinear acoustic scattering of waves is important for generating the low-frequency response of

DOI: 10.6061/clinics/2013(04)05

objects in VA (9-11). The different frequencies are detected by a hydrophone that is coupled to the system. The focused low-frequency excitation provides a speckle-free image with a high (sub-mm) lateral resolution. The feasibility of VA has been demonstrated for evaluating soft tissues, such as arteries (12,13), breast tissue (14,15), and prostate tissue (16). However, the implementation of VA in a commercial machine (17) and the development of new technologies for VA beam forming (18) open a new range of clinical applications.

An important property of VA is its relative insensitivity to the sound beam orientation with respect to the object, which allows VA to image specular surfaces with high local curvatures of bone and metal implants. This characteristic is an important advantage of VA over traditional B-mode ultrasound imaging, which often misses a signal if the object surface is not perpendicular to the beam. Barratt et al. (19) described a 3D system composed of a B-mode ultrasound imaging system and an optical tracking device for pelvic bone imaging. The authors reported some difficulties associated with this technique for imaging complex anatomic structures with high curvatures. A comparative study between VA and B-mode (pulse-echo) ultrasound for brachytherapy seed imaging showed that the image quality in VA was far less affected by the orientation of seeds for the range up to 80° than the images acquired in B-mode (20). B-mode ultrasound is highly affected by angle variation because the image formation in this technique is based on reflected wave intensity. At incidence angles greater than a few degrees, the reflected ultrasound beam mostly misses the transducer, which significantly decreases the reflected wave intensity that the transducer can receive. In VA, a hydrophone is used to acquire the tissue response under low-frequency excitation. The low-frequency wave is propagated in all directions, and its attenuation is much less than the attenuation at high frequencies. Therefore, the orientation of the object and the hydrophone position are not critical for VA acquisition. The low variability in the VA image in relation to the incidence angle is particularly important in this study because the bone and cup surfaces may have great variations in shape.

Calle et al. (21) presented the VA technique for bone imaging and showed the trabecular structure of a cut calcaneus bone. The authors used low ultrasound frequencies that penetrate deeper the tissue to observe internal structures of the bone. Renaud et al. (22) reported preliminary results for a heel bone crack assessment using ultrasound excitation, including VA. Moreover, Alizad et al. (23) presented a frequency spectrum analysis of fractured bones.

In the study presented here, we propose VA imaging with 3D correction of the topology for evaluating the uncovered cup surface area in THA. For an accurate evaluation of the surface area, an analytic correction based on the 3D geometry of the implant (cup) was made to the VA image to generate a 3D representation of it. Furthermore, an optical measurement was conducted to provide an independent measurement of the uncovered area.

MATERIALS AND METHODS

The THA Model

A hemispherical acetabular implant cup with an outer diameter of 57.10 ± 0.05 mm was placed inside a pelvic bone model to simulate THA. The bone model (Sawbones Model 1301-1, Pacific Research Laboratories, Inc., Vashon, Washington, USA) was made of foam cortical shell material and had the dimensions of a typical adult pelvis and an elastic modulus of 210 MPa. The uncovered surface area, shown in Figure 1, was evaluated for cup fixation. A tissue-mimicking material (TMM) was placed between the THA model and the ultrasound transducer to simulate muscle and fat in the buttock region. To ensure a more realistic TMM, the damping effect of the wave was considered, and the TMM was molded to conform to the shape of the bone and implant surfaces, and placed in contact with these structures. The TMM was composed of water (50% of the volume), evaporated milk (approximately 50% of the volume), porcine skin–derived gel (180 g), glycerol (180 mL), and potassium sorbate (18 g). The TMM attenuation was controlled by diluting the evaporated milk in water (24). The tissue phantom exhibited attenuation of approximately 0.5 $dB \cdot cm^{-1}$, a propagation speed of 1540 $m \cdot s^{-1}$, and a 5-cm thickness. The empirical values for the attenuation coefficients of fat and skeletal muscles were previously reported by Mast (25). The resultant attenuation coefficient of the TMM was similar to a muscle to fat proportion of 2 to 3.

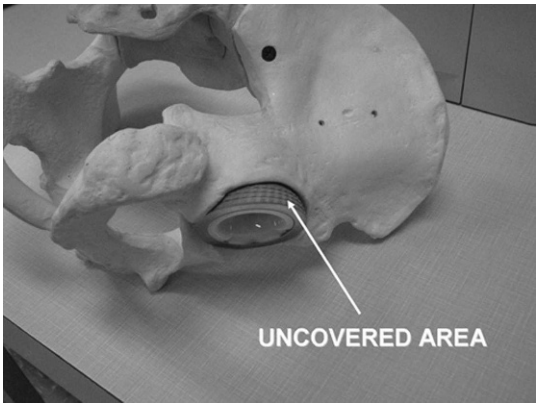

Figure 1 - Total hip arthroplasty model. The metal implant was positioned inside the pelvis. The uncovered area was evaluated using vibroacoustography.

Uncovered Implant Area Estimation

The boundary of the uncovered surface area was digitized using a motion capture system (OptotrakCertus; NDI, Inc. Waterloo, Ontario, Canada). The area was calculated using computer-aided design (CAD) software (SolidWorks; Dassault Systèmes S.A., Vélizy, France), which provided an accuracy of 0.15 mm at 2.25 m of distance between the system and the THA model.

The pelvic model was positioned on a rigid table, which was stationary in relation to the optical system. Using the marker digitizing probe, the diameter of the implant was determined by acquiring six points on the edge of the implant. Those points represented the external implant diameter and were used to build the sphere surface model with the CAD software. Next, 20 points on the border of the uncovered implant area were acquired to determine the region of interest (ROI). A 3D curve, which was defined by the ROI points, was used to define the uncovered area on the sphere surface. The uncovered area was calculated using the surface area evaluation tool of the CAD software.

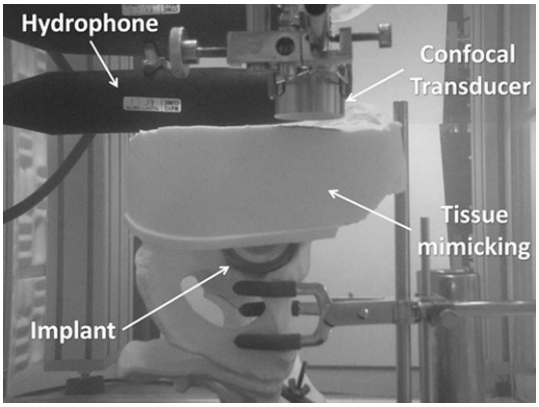

Figure 2 - Vibroacoustography image acquisition using a confocal ultrasound transducer and a tissue-mimicking gel to simulate the soft tissue around the hip.

VA Acquisition

The VA acquisition was performed inside a tank of degassed water. A confocal ultrasound transducer with an outer diameter of 45 mm and a focal distance of approximately 7 cm was positioned with a 3-axis scanner system (0.25-mm resolution) and swept the pelvic model in a 5×7-cm raster pattern. The implant face of the THA model was oriented parallel to the transducer scan axis (Figure 2).

The focal depth of the transducer was approximately 1 cm long. With this focal depth and the amount of curvature of the implant's surface, the uncovered area of the implant could not be covered by the focal region in only 1 scanning plane. Thus, three acquisition planes at depths of 5.3 cm, 5.8 cm, and 6.3 cm from the transducer were acquired and combined into one image to extend the focal depth coverage to the entire exposed implant area.

Image Processing

The VA images were combined with equal weightings using the linear combination of the images shown in Figure 3. The surface area of the VA image was automatically identified by contour segmentation on the basis of gradient-based edge detection (26). Analytic topology correction was performed to obtain 3D representations of the VA image. Finally, the uncovered area was evaluated using the 3D surface representations.

Contour Segmentation

The uncovered implant area was identified by analyzing the image texture using contour detection (27). The gradient magnitude of the image was computed to detect the image edges. The edges were characterized by sudden changes in the gray level, and they were defined by evaluating the partial derivative with respect to the x and y directions.

The Sobel edge masks were used to calculate the horizontal and vertical gradient magnitude (the vertical gradient magnitude was calculated by transposing the filter). The square root of the sum of the squared gradients in both directions was evaluated, providing the image shown in Figure 4(b).

Next, a threshold was applied to the image followed by operations to dilate and fill the holes in the ROI. The segmented area had a high brightness and is highlighted in Figure 4(d).

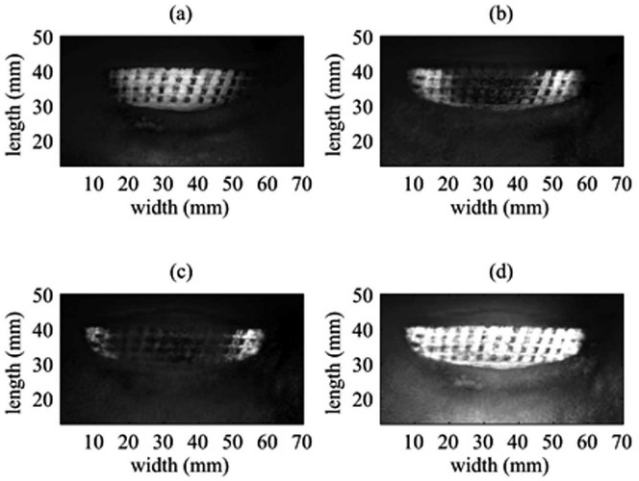

Figure 3 - Linear combination of vibroacoustography images at three different depths: (a) VA image at a depth of 6.3 cm, (b) VA image at a depth of 5.8 cm, (c) VA image at a depth of 5.3 cm, and (d) a linear combination of the images with equal weighting. The cross-hatch texture of the image is caused by tiny elevated squares on the implant surface.

Topology Correction

For an accurate evaluation of the uncovered area, a correction in the topology of the image was necessary because the combined VA image used here was only 2-dimensional. An analytic approach for the topology correction was performed based on the implant cup dimensions. In this approach, the topology of the 3D implant surface was given by a quarter of a sphere.

For the 3D visualization of the uncovered area, the VA image was applied as a texture on the 3D surface (topology). The segmented region in Figure 4(c) defined the uncovered area to be evaluated on the 3D surface.

Surface Area Evaluation

The total surface area of the implant was estimated by calculating the surface area of half of a sphere, equal to

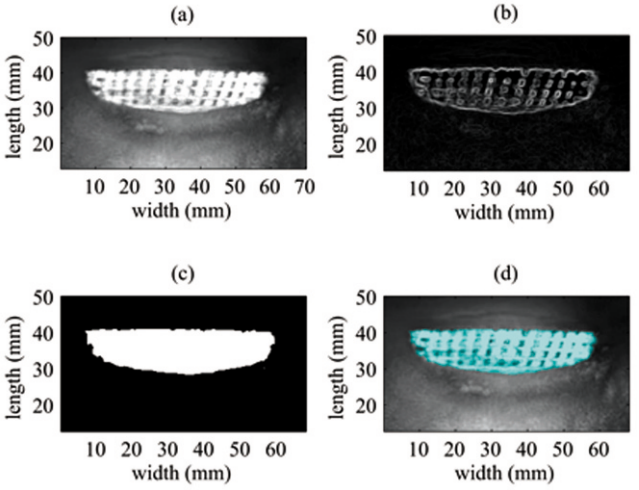

Figure 4 - Contour segmentation in the image acquired by the vibroacoustography technique: (a) the combined image, (b) the gradient magnitude, (c) the segmented region, and (d) the highlighted segmented area on the image.

$2 \cdot \pi \cdot r^2$, where r is the radius of the sphere. After the topology corrections were applied, the segmented area in the VA image defined the surface area to be evaluated. The surface area was numerically computed by calculating the sum of the triangular subareas formed by three neighbor pixels. The x, y, and z coordinates of the points (pixels) determined the 3D surface in space; these coordinates represented the vertices of the triangles. The subareas (of the triangles) were calculated by the cross-product of the vectors defined by the vertices (28). The accuracy of the numeric area evaluation depended on the number of pixels. The resolution in the acquisition was set to 0.25 mm/pixel, which allowed for highly accurate results.

The proposed method is diagrammed in Figure 5, which shows the steps for evaluating the implant uncovered area.

RESULTS

The metal implant diameter was 5.71 cm, and the total surface area was 51.2 cm^2. The estimated uncovered area determined by the optical measurements was 6.64 cm^2 and represented 13.0% of the implant surface area.

The uncovered area in the VA image was detected by contour segmentation. The image had a high contrast between the metal and bone, which revealed considerable surface detail. Using the analytical approach to correct the surface topology, as shown in Figure 6(a), the uncovered area was found to be 6.10 cm^2, which represented 11.9% of the implant surface area.

DISCUSSION

VA is an imaging technique that can be used *in vivo* for soft tissue evaluation. This study presented a new clinical application for VA for evaluating THA. Differences in the mechanical properties of objects, such as stiffness, density, acoustic impedance, and shape, determine the contrast and resolution of the image. In addition, low and high frequencies interact differently with metal and bone. In VA, differences in the mechanical properties of bone and metal, including absorption, scattering, and stiffness, provide high contrast between the bone and implant. In the VA modality, the low-frequency response is less affected by changes in the incidence angle of the ultrasound beam with respect to the specular surfaces of the bone or implant. This feature of VA imaging contrasts with B-mode imaging. For B-mode imaging, the echo signal level strongly depends on the beam angle with respect to the object surface, which negatively impacts image quality. Our results showed that the good contrast of VA images facilitated the segmentation process of the uncovered region. In this study, we used an optical method to provide an independent measurement of the 3D uncovered surface area. Although this optical method offers high accuracy (0.15 mm) for point acquisition, the manual handling of the optical probe may introduce additional error into the measurements and requires care with use. In our experiments, the optical measurements of the percentage of the uncovered area were similar to those obtained by VA, and the relative error was 8.1%. The agreement between the two methods supports the validity of the VA approach for *in vivo* applications. Further research is necessary to make a statistical conclusion about the mean error and to demonstrate the application in humans.

The calculated surface area was simplified using the priori knowledge of implant geometry. Because the implant dimensions are known in clinical THA, analytical correction of the topology can be easily applied to the VA image of the implant. Because of the spherical symmetry of the implant model, the alignment of the VA image is easily reached by aligning the midpoint on top of the implant with the equivalent point on the 3D analytic topology. Thus, even when the VA image is acquired at an arbitrary orientation with respect to the implant, angle alignment of the VA image in the xy plane (length and width plane) is not necessary to correctly evaluate the uncovered area. This property further facilitates the clinical application of this technique.

Overall, the results of this study support the feasibility of VA to postoperatively evaluate THA and its potential as a noninvasive alternative to x-ray–based methods that use ionizing radiation. The quality of the images also suggests that VA may be a practical solution for evaluating implants

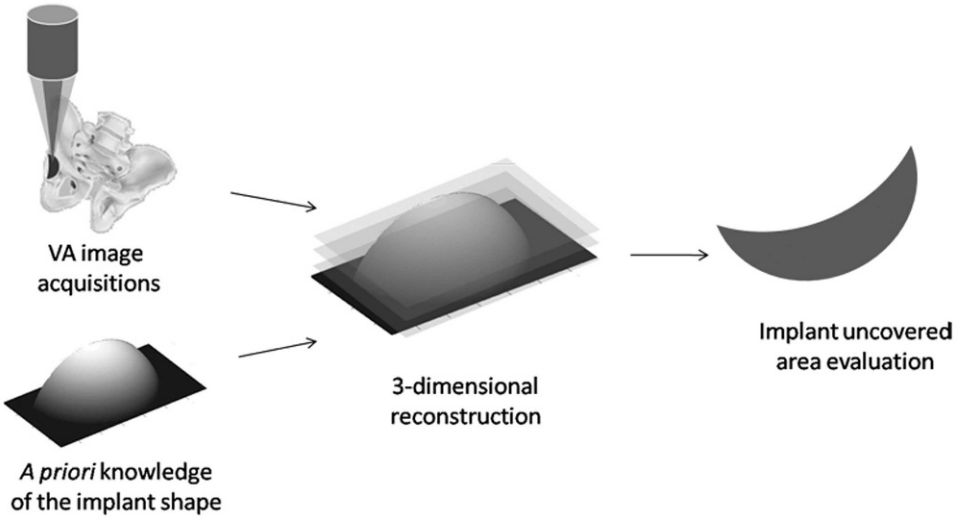

Figure 5 - Schematic showing the steps for the implant uncovered area evaluation. The VA images were acquired and combined into one image. The uncovered implant area was determined by a segmentation process. The resulting image was fitted to a priori known shape of the implant to account for the curvature of the 3D shape of the uncovered area.

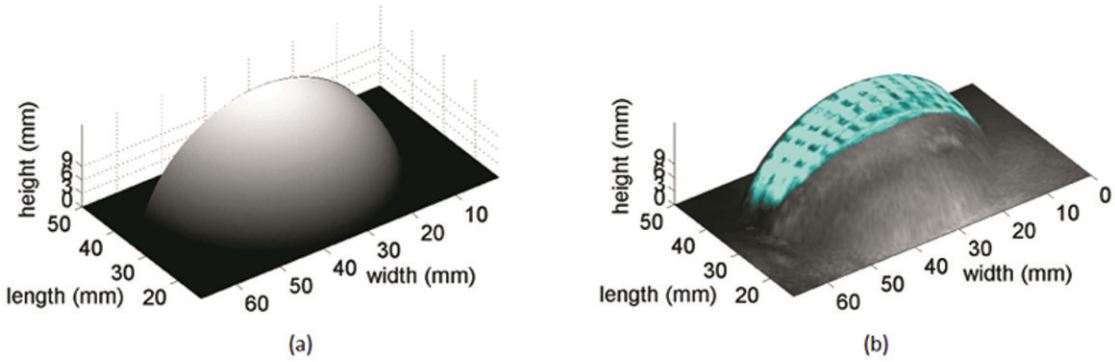

Figure 6 - A 3D representation of the implant topology using the analytic approach: (a) analytic topology and (b) 3D image result.

designed for shallower regions, such as the arms and knees. The favorable results of this study also provide the impetus for further research of other application areas, such as diagnostic bone surface imaging and *in vivo* imaging of metallic implants in other parts of the body. The range of applications may also be broadened by using more sophisticated methods, which would improve image resolution and contrast, and lower image distortion, to restore VA images (29).

Conflicts of Interest: Mayo Clinic and one of the authors (Fatemi M) have financial interests associated with the technology used in this research, and the technology has been licensed (in part) to industry.

■ ACKNOWLEDGMENTS

This work was supported in part by the Brazilian agencies CNPq (process: 571801/2008-0) and FAPESP (process: 2011/10809-6). The authors thank James F. Greenleaf, PhD, Matthew W. Urban, PhD, and Thomas M. Kinter for their assistance in the technical discussions and with image processing.

■ AUTHOR CONTRIBUTIONS

All of the co-authors have read the manuscript and contributed substantially to it. This work was partially conducted while Kamimura HA was visiting a graduate student and Wang L was a fellow at the Mayo Clinic (2010/2011). Kamimura HA, Wang L, and Kinnick RR worked on the experiments together. Wang L and An KN designed the realistic problem to better represent the clinical problem. Kamimura HA, Fatemi M, and Carneiro AA discovered the solution to build the 3D image and worked on the image processing.

■ REFERENCES

1. Anderson MJ, Harris WH. Total hip arthroplasty with insertion of the acetabular component without cement in hips with total congenital dislocation or marked congenital dysplasia. J Bone Joint Surg Am. 1999;81A(3):347-54.
2. Hartofilakidis G, Georgiades G, Babis GC, Yiannakopoulos CK. Evaluation of two surgical techniques for acetabular reconstruction in total hip replacement for congenital hip disease - Results after a minimum ten-year follow-up. J Bone Joint Surg British. 2008;90B(6):724-30, http://dx.doi.org/10.1302/0301-620X.90B6.20490.
3. Jasty M, Anderson MJ, Harris WH. Total hip-replacement for developmental dysplasia of the hip. Clin Orthop Relat Res. 1995;311:40-5.
4. Kim YH, Seo HS, Kim JS. Outcomes after THA in patients with high hip dislocation after childhood sepsis. Clin Orthop Relat Res. 2009;467(9):2371-8, http://dx.doi.org/10.1007/s11999-008-0654-0.
5. Sanchez-Sotelo J, Trousdale RT, Berry DJ, Cabanela ME. Surgical treatment of developmental dysplasia of the hip in adults: I. Nonarthroplasty options. J Am Acad Orthop Surg. 2002;10(5):321-33.
6. Dean LW. Interactions between sound waves. J Acoust Soc Am. 1962;34(8):1039-44, http://dx.doi.org/10.1121/1.1918241.
7. Fatemi M, Greenleaf JF. Ultrasound-stimulated vibro-acoustic spectrography. Science. 1998;280(5360):82-5, http://dx.doi.org/10.1126/science.280.5360.82.
8. Fatemi M, Greenleaf JF. Vibro-acoustography: An imaging modality based on ultrasound-stimulated acoustic emission. Proc Nat Acad Sci USA. 1999;96(12):6603-8, http://dx.doi.org/10.1073/pnas.96.12.6603.
9. Silva GT, Mitri FG. Analysis of the difference-frequency wave generated by the interaction of two axisymmetric and co-focused ultrasound beams, in: Proc. IEEE Ultrason. Symp., IEEE-UFFC, 2008.pp.1326-9.
10. Silva GT, Farid FG. Difference-frequency generation in vibro-acoustography. Phys. Med. Biol. 2011;56(18):5985-93, http://dx.doi.org/10.1088/0031-9155/56/18/013.
11. Bandeira A, Silva GT. Difference-frequency generation in nonlinear scattering of acoustic waves by a rigid sphere. Ultrasonics. 2013;53(2):470-8.
12. Alizad A, Fatemi M, Whaley DH, Greenleaf JF. Application of vibro-acoustography for detection of calcified arteries in breast tissue. J Ultrasound Med. 2004;23(2):267-73.
13. Pislaru C, Kantor B, Kinnick RR, Anderson JL, Aubry MC, Urban MW, et al. In vivo vibro-acoustography of large peripheral arteries. Invest Radiol. 2008;43(4):243-52, http://dx.doi.org/10.1097/RLI.0b013e31816085fc.
14. Fatemi M, Wold LE, Alizad A, Greenleaf JF. Vibro-acoustic tissue mammography. IEEE Trans Med Imaging. 2002;21(1):1-8, http://dx.doi.org/10.1109/42.981229.
15. Alizad A, Whaley DH, Urban MW, Carter RE, Kinnick RR, Greenleaf JF, et al. Breast vibro-acoustography: initial results show promise. Breast Cancer Research. 2012;14(5):R128, http://dx.doi.org/10.1186/bcr3323.
16. Mitri FG, Trompette P, Chapelon JY. Improving the use of vibro-acoustography for brachytherapy metal seed imaging: A feasibility study. IEEE Trans Med Imaging. 2004;23(1):1-6, http://dx.doi.org/10.1109/TMI.2003.819934.
17. Urban MW, Chalek C, Kinnick RR, Kinter TM, Haider B, Greenleaf JF, et al. Implementation of vibro-acoustography on a clinical ultrasound system. IEEE Trans Ultrason Ferroelectr Freq Control. 2011;58(6):1169-81, http://dx.doi.org/10.1109/TUFFC.2011.1927.
18. Kamimura HAS, Urban MW, Carneiro AAO, Fatemi M, Alizad A. Vibro-acoustography beam formation with reconfigurable arrays. IEEE Trans Ultrason Ferroelectr Freq Control. 2012;59(7):1421-31, http://dx.doi.org/10.1109/TUFFC.2012.2343.
19. Barratt DC, Chan CSK, Edwards PJ, Penney GP, Slomczykowski M, Carter TJ, et al. Instantiation and registration of statistical shape models of the femur and pelvis using 3D ultrasound imaging. Medical Image Analysis. 2008;12(3):358-74, http://dx.doi.org/10.1016/j.media.2007.12.006.
20. Mitri FG, Davis BJ, Greenleaf JF, Fatemi M. In vitro comparative study of vibro-acoustography versus pulse-echo ultrasound in imaging permanent prostate brachytherapy seeds. Ultrasonics. 2009;49(1):31-38, http://dx.doi.org/10.1016/j.ultras.2008.04.008.
21. Calle S, Remenieras JP, Matar OB, Defontaine M, Patat F. Application of nonlinear phenomena induced by focused ultrasound to bone imaging. Ultrasound Med Biol. 2003;29(3):465-72, http://dx.doi.org/10.1016/S0301-5629(02)00729-9.
22. Renaud G, Calle S, Remenieras JP, Defontaine M. Non-linear acoustic measurements to assess crack density in trabecular bone. Int J Non-Linear Mech. 2008;43(3):194-200, http://dx.doi.org/10.1016/j.ijnonlinmec.2007.12.007.
23. Alizad A, Wallch M, Greenleaf JF, Fatemi M. Vibrational characteristics of bone fracture and fracture repair: Application to excised rat femur. J Biomech Eng. 2006;128(3):300-8, http://dx.doi.org/10.1115/1.2187037.
24. Madsen EL, Frank GR, Dong F. Liquid or solid ultrasonically tissue mimicking materials with very low scatter. Ultrasound Med Biol. 1998;24(4):535-42, http://dx.doi.org/10.1016/S0301-5629(98)00013-1.
25. Mast TD. Empirical relationships between acoustic parameters in human soft tissues. Acoustics Research Letters Online. 2000;1(2):37-42, http://dx.doi.org/10.1121/1.1336896.
26. Burger W, Burge MJ. Digital image processing: an algorithmic introduction using Java. 1st ed. New York: Springer-Verlag New York Inc; 2008.

27. Pal NR, Pal SK. A review on image segmentation techniques. Pattern Recognition. 1993;26(9):1277-94, http://dx.doi.org/10.1016/0031-3203(93)90135-J.
28. Zill DG, Wright WS. Advanced engineering mathematics, 10th ed. Massachusetts: Jones and Bartlett Publishers Inc; 2006.
29. Perciano T, Urban MW, Mascarenhas NDA, Fatemi M, Frery AC, Silva GT. Deconvolution of vibroacoustic images using a simulation model based on a three dimensional point spread function. Ultrasonics. 2013;53(1):36-44, http://dx.doi.org/10.1016/j.ultras.2012.03.011.